Vol. 20 (2026): Proceedings of 2026 International Conference on Materials Science, Energy Engineering and Automation Control (ICMSEAC 2026)
E-ISSN: 3105-0522 P-ISSN: 3105-0514
DOI: https://doi.org/10.70267/mseac.2026200210

Low-carbon Optimal Scheduling of Electric Vehicles With High Spatiotemporal Resolution

Zicen Chang*
School of Electrical and Electronic Engineering, Nanyang Technology University, Singapore
**Corresponding author: Zicen Chang.*

Abstract

As electric vehicles (EVs) become increasingly connected to power systems at scales, their emission reduction benefits no longer depend merely on whether the vehicles themselves are zero-emission, but are also closely related to charging time, charging location, and the carbon intensity of electricity sources. In order to reduce indirect carbon emissions of charging for EVs, a user-side low-carbon optimal scheduling framework for EVs is established, in which dynamic electricity pricing, energy storage system operation, charging characteristics of various EV types and dynamic carbon emission factor are considered. Firstly, based on the carbon emission approach, user-side electricity consumption behavior is associated with nodal carbon intensity, which provides a theoretical basis for evaluating the carbon footprint of EVs. Secondly, through dynamic pricing mechanisms and real-time electricity trading prices, electric vehicles are encouraged to charge during low-load or low-carbon periods, while energy storage systems are coordinated for charging and discharging operations to improve the peak-to-valley load profile. Lastly, experiments are conducted to analyze the variation patterns of optimized electricity price curves, categorized EV charging power behaviors, storage system operating conditions, and the variations in dynamic marginal carbon emission factors and overall carbon emission factors. The experimental results indicate that electricity price signals alone are insufficient for user-side low-carbon scheduling, and that dynamic carbon emission factors should also be taken into account.

Keywords

carbon emission flow, dynamic carbon emission factor, electric vehicles, energy storage system, low-carbon scheduling

1. Introduction

In recent years, as transportation electrification and the transition toward low-carbon energy systems continue to accelerate, electric vehicles (EVs) have been widely recognized as an important solution for reducing carbon emissions in the transportation sector. Compared to conventional fuel vehicles, electric vehicles emit virtually no direct exhaust gases during driving, thereby offering considerable advantages in improving urban air quality and reducing dependence on fossil fuels. However, the low-carbon benefits of EVs are not absolute. If the electricity used for charging is mainly generated from high-carbon energy sources such as coal-fired power plants, the carbon emissions reduced on the transportation side may instead be shifted to the electricity sector as indirect emissions. As a result, the core issue of low-carbon EV scheduling is not merely the adoption of electric vehicles, but also the timing, location, and energy source of charging.

Current research shows that low-carbon optimization and scheduling of user-side EVs primarily focuses on carbon flow tracking, modeling of user charging behaviors, dynamic pricing and carbon trading incentive schemes, and vehicle-to-grid (V2G) interaction. Carbon flow tracing theory enables carbon emissions generated at the power generation side to be allocated to the load side along power flow paths, thereby allowing the calculation of nodal carbon potential or nodal carbon intensity and providing a basis for quantifying user-side carbon responsibility. Existing review studies indicate that nodal carbon potential reflects the carbon emission intensity associated with electricity consumption per unit of energy at a node, while the carbon emissions of flexible loads such as electric vehicles can be further determined jointly by charging or discharging power and nodal carbon potential [1-4].

On this basis, dynamic pricing, multi-level carbon pricing, and carbon trading schemes can encourage users to modify their charging patterns through economic signals, thereby achieving both load shifting and carbon emission reduction. Some previous research has shown that the synergy between dynamic electricity pricing and carbon trading mechanisms can encourage EV charging to move from peak-demand periods to periods characterized by lower load and lower carbon potential, which decreases user charging expenses and overall system carbon emissions. Although existing studies have explored the issue of low-carbon scheduling for electric vehicles from different perspectives, certain shortcomings still exist in the current literature. Firstly, existing research tends to emphasize low-carbon optimization on the generation or system side, with limited consideration given to the diversity of user-side charging behaviors. In practice, different types of EV users exhibit significant differences in charging time, charging power, and price responsiveness, which directly affect power grid load profiles and carbon emission levels. Secondly, many existing scheduling strategies depend mainly on electricity pricing signals, but periods of low electricity prices are not necessarily characterized by low carbon emissions. Due to the significant variability of renewable energy outputs such as photovoltaic and wind power, the system marginal carbon emission factor changes over time. Hence, charging optimization conducted solely according to electricity prices may not guarantee actual low-carbon performance. Furthermore, energy storage systems play a significant role in load balancing and renewable energy accommodation, yet the coupling relationships among storage operation, EV charging patterns, real-time pricing, and dynamic carbon emission factors still need further analysis [5-10].

Based on the limitations identified above, this paper investigates user-side low-carbon optimal scheduling of electric vehicles and develops an analytical framework that integrates dynamic electricity pricing, energy storage operation, classified EV charging behaviors, and dynamic carbon emission factors. From a theoretical perspective, this paper first clarifies the relationships among carbon emission flow, nodal carbon intensity, EV carbon footprint, and vehicle-grid interaction. Afterwards, simulation cases are established in the experimental section to study the changing trends of optimized electricity tariffs, EV charging power, storage charging or discharging operations, real-time electricity market prices, and dynamic marginal as well as integrated carbon emission factors.

By comparing the relationships among different curves, this study seeks to show that user-side low-carbon scheduling should consider both economic performance and carbon emission characteristics, instead of using minimum electricity prices alone as the criterion for charging decisions.

In summary, the key contributions of this study are outlined in the following three aspects. Firstly, a user-side low-carbon scheduling analysis framework for electric vehicles is proposed, which integrates electricity price signals, energy storage operation, and carbon emission factors. Secondly, this study takes into account the charging behavior differences of different EV types and investigates their effects on load transfer and scheduling performance. Thirdly, the relationships between dynamic electricity pricing, energy storage behavior, and carbon emission factors are examined through experimental results, confirming the necessity of incorporating both price and carbon signals into low-carbon scheduling.

2. Framework

The carbon emission flow (CEF) model was first introduced to trace the carbon footprint from the generation side to the demand side based on the proportional sharing principle, thereby achieving allocation of carbon emissions to consumers [1-3].

The primary motivation for developing an emission-tracing model is to achieve a comprehensive and accurate assessment of the indirect emissions associated with the production and utilization of electric vehicles (EVs). Unlike supply-side emission control, the key rationale for demand-side management is to fully account for EVs' environmental impact. Although EVs produce zero direct emissions during driving, significant indirect emissions arise from battery manufacturing and electricity production. By tracing emissions from the demand side, it becomes possible to quantify the complete environmental footprint of EVs, identify opportunities for improvement, and ensure that the adoption of EVs delivers substantial benefits in terms of greenhouse gas (GHG) reduction and enhanced energy efficiency.

In a power system, the power balance equation can be expressed as follows [1, 2]:

$$\rho = \frac{R}{P} \tag{1}$$

$$\bar{\rho} = \frac{\int R\mathrm{d}\ t}{\int P\mathrm{d}\ t} = \frac{F}{Q} \tag{2}$$

$$e_n = \frac{\sum_{i\in N^+} P_i\rho_i}{\sum_{i\in N^+} P_i} = \frac{\sum_{i\in N^+} R_i}{\sum_{i\in N^+} P_i} \tag{3}$$

$$\frac{P_{j,i}}{P_j} = \frac{P_i}{\sum_{s\in N^+} P_s} \tag{4}$$

$$R_j = \sum_{i\in N^+} P_{j,i}\,\rho_i \tag{5}$$

$$\rho_j' = \frac{R_j}{P_j} = \frac{\sum_{i\in N^+} P_{j,i}\rho_i}{P_j} \tag{6}$$

$$P_{j,i} = P_j \frac{P_i}{\sum_{s\in N^+} P_s} \tag{7}$$

$$\rho_j' = \frac{\sum_{i\in N^+} P_i \frac{P_i}{\sum_{s\in N^+} P_s}\rho_i}{P_j} = \frac{\sum_{i\in N^+} P_i\rho_i}{\sum_{s\in N^+} P_s} = \frac{\sum_{s\in N^+} R_s}{\sum_{s\in N^+} P_s} = e_n \tag{8}$$

where ρ represents the carbon intensity or carbon emission intensity, which defines the amount of CO_2 emitted per unit of energy or product, such as kg CO_2/kWh; R denotes the total carbon emissions, which represent the absolute quantity of emissions associated with a specific process or period; P denotes the power flow or production output, which typically refers to active power in power systems and total energy or material throughput in industrial contexts; $\bar{\rho}$ is the time-average carbon intensity, which is calculated as the ratio of cumulative emissions F to total energy produced or consumed Q over a specific time interval; ρ_i represents the carbon intensity of source i, which is weighted by its share of the total power P; P_{ij} represents the component power allocation, which refers to the portion of the total power at node j supplied by source i; R_j is the allocated carbon footprint of consumer or subsystem j, which is calculated by summing the products of each energy component and its corresponding carbon intensity; ρ_j is the equivalent carbon intensity of subsystem j, which represents the effective carbon intensity associated with that subsystem; and Ω_j denotes the set of inflow sources or generators, which contribute to the energy supply of subsystem j.

Carbon intensity physically represents the amount of CO_2 emitted per unit of electricity consumed. Lower values indicate cleaner and more efficient generation processes, while higher values reflect greater pollution. Equation essentially computes the ratio of total carbon injection to total power injection.

However, the traditional CEF model does not account for energy storage systems (ESS). To incorporate ESS, an adjustment of the model is made. ESS operates in three states: charging, discharging, or idle. In the idle state, carbon intensity remains unchanged. During charging, ESS acts as a load absorbing grid energy, so its carbon intensity is influenced by that of the absorbed electricity. When discharging, ESS behaves as a generator, and its carbon intensity stays constant. Then as a result, the following nodal carbon intensity evolution equation for ESS is proposed:

$$e_{\mathrm{N}i} = \frac{\sum_{s \in I^+} p_{\mathrm{B}s} \rho_s + p_{\mathrm{G}i} e_{\mathrm{G}i}}{\sum_{s \in I^+} p_{\mathrm{B}s} + p_{\mathrm{G}i}} \tag{9}$$

$$e_{\mathrm{N}i} = \frac{\boldsymbol{\eta}_N^{(i)} \left(\boldsymbol{P}_{\mathrm{B}}^{\mathrm{T}} \boldsymbol{E}_{\mathrm{N}} + \boldsymbol{P}_{\mathrm{G}}^{\mathrm{T}} \boldsymbol{E}_{\mathrm{G}} \right)}{\sum_{v=1}^{N} P_{\mathrm{B}vi} + \sum_{t=1}^{K} P_{\mathrm{G}ti}} \tag{10}$$

$$E_D = AD \times EF \tag{11}$$

$$MCI_n = \frac{\partial C}{\partial P_n} \tag{12}$$

$$\sum_{v=1}^{N} P_{\mathrm{B}vi} + \sum_{t=1}^{K} P_{\mathrm{G}ti} = \eta_N^{(i)} P_{\mathrm{N}} (\eta_N^{(i)})^{\mathrm{T}} \tag{13}$$

$$\eta_N^{(i)} P_N (\eta_N^{(i)})^{\mathrm{T}} e_{Ni} = \eta_N^{(i)} (P_{\mathrm{B}}^{\mathrm{T}} E_{\mathrm{N}} + P_{\mathrm{G}}^{\mathrm{T}} E_{\mathrm{G}}) \tag{14}$$

$$P_{\mathrm{N}} E_{\mathrm{N}} = P_{\mathrm{B}}^{\mathrm{T}} E_{\mathrm{N}} + P_{\mathrm{G}}^{\mathrm{T}} E_{\mathrm{G}} \tag{15}$$

$$E_{\mathrm{N}} = (P_{\mathrm{N}} - P_{\mathrm{B}}^{\mathrm{T}})^{-1} P_{\mathrm{G}}^{\mathrm{T}} E_{\mathrm{G}} \tag{16}$$

where $e_{\mathrm{N}i}$ represents the Node Carbon Intensity (or Carbon Potential) at node i, which is the average emission factor of the power passing through that specific node; $\mathrm{p}_{\mathrm{B}s}$ and $P_{\mathrm{B}vi}$ denote the Branch Power Flow (or line flow) entering node i from other nodes in the network; ρ_s is the Carbon Intensity of the Power Flow on branches entering the node; $P_{\mathrm{G}i}$ and $P_{\mathrm{G}ti}$ represent the Power Injected by Generators directly connected to node i; $e_{\mathrm{G}i}$ denotes the Carbon Emission Intensity of the Generator at node i, based on its fuel type and efficiency; E_{N} is the Node Carbon Intensity Vector containing the carbon intensities for all nodes in the system; E_{G} is the Generator Carbon Intensity Vector representing the specific emissions of all generators in the network; P_{N} is the Diagonal Matrix of Node Throughput Power, where each diagonal element represents the total power flux at a specific node; $P_{\mathrm{B}}^{\mathrm{T}}$ is the Transpose of the Branch Power Matrix representing the network topological connections and power flow magnitudes between nodes; $P_{\mathrm{G}}^{\mathrm{T}}$ is the Transpose of the Generator Power Matrix mapping generator outputs to their respective nodes; $\eta_{\mathrm{N}}^{(i)}$ is an Incidence/Selection Vector used to extract values related to a specific node i from the system matrices; ED represents the direct carbon emissions resulting from fuel consumption; AD refers to the activity data representing the specific use and input quantity of a single emission source directly linked to carbon emissions; EF is the emission factor obtained from various sources; MCI_n is the marginal carbon intensity of node n; C denotes the power system carbon emissions; and P_n is the load of node n.

A microgrid consists of various electrical energy sources and loads that can operate autonomously using distinct control algorithms within a power system. It is typically capable of synchronizing with the traditional centralized grid. Although it can function either respectively or in grid-connected mode, it essentially represents a scaled-down version of the conventional power grid [11].

The intermittent nature of renewable energy sources such as solar and wind can be effectively managed in the short term by storing additional energy in electric vehicles (EVs) and discharging it during periods of need. The growing integration of EVs into the transportation sector will require substantial modifications to microgrid operation and control strategies. These changes have the potential to simplify frequency regulation during peak load periods and contribute to a reduction in greenhouse gas emissions [12-14].

Figure 1: Proposed microgrid and EV aggregation framework

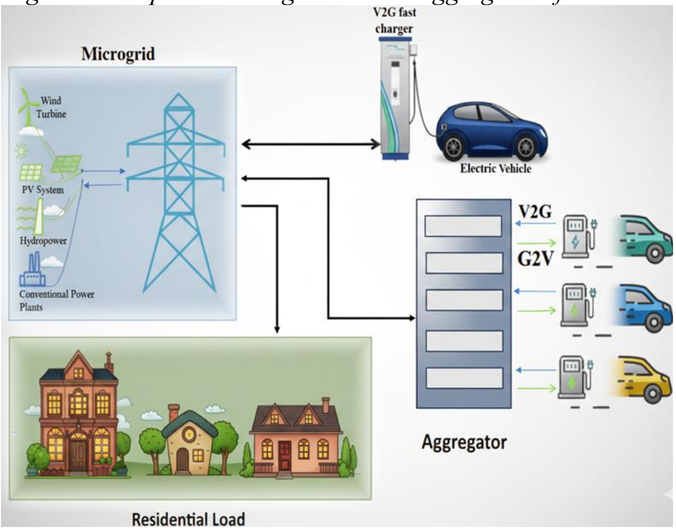

The proposed model is designed to enable the microgrid to operate either independently or in parallel with the main utility grid. Renewable energy resources, including solar photovoltaic (PV) panels and wind turbines, can be incorporated to generate electricity whenever they are available. In cases where renewable generation is inadequate, waste-to-energy plants and conventional power stations serve as reliable backup sources. An aggregator is employed to continuously monitor and balance energy supply and demand within the microgrid, while also allowing the microgrid to deliver power to residential consumers.

In this structure (see Figure 1), an electric vehicle aggregator performs frequency regulation services by receiving control signals from the central control center, which indicate the need to raise or lower system frequency. Within the system, electrical energy is shared among the microgrid, the main grid, and the connected EVs, with overall management handled by the aggregator. The aggregator also oversees the charging and discharging processes of EV batteries. Consequently, the microgrid is able to supply electricity to residential loads by drawing power from EV batteries, solar PV systems, and other available primary energy sources.

Electric vehicles produce no direct carbon emissions, but indirect emissions arise from charging if the electricity is not sourced from renewables. Carbon footprint tracking for EVs can be achieved using the CEF model, where indirect emissions equal the product of EV charging power and the nodal carbon intensity at the corresponding location:

$$CE^{EV} = e_{i,t}^{N} P_{i,t}^{EV} \Delta t \tag{17}$$

Under the probabilistic CEF (PCEF) model, the expected carbon emissions from EV charging are constrained as: (Qiu et al., 2016)

$$\sum_{i}\sum_{t} \mathbb{E}[e_{i,t}^{N(n)}] P_{i,t}^{EV} \Delta t \le M_1 \tag{18}$$

where $M_1 M_1$represents the indirect emission cap for EVs.

Furthermore, a chance-constrained carbon footprint cap criterion for EVs can be formulated as:

$$\Pr\left(\sum_{i}\sum_{t} e_{i,t}^{N} P_{i,t}^{EV} \Delta t \le M_2\right) \ge \kappa \tag{19}$$

Equation (19) indicates that the likelihood of the indirect emissions attributable to electric vehicles (EVs) remaining below the threshold $M_g M_g$ should be bigger than $\kappa\kappa$.

In both equations (18) and (19), $P_{i,t}^{EV} P_{i,t}^{EV}$ must be further estimated. EV charging is typically conducted through three primary modes: fast-charging stations (FCS), charging posts (CP), and residential wall outlets. While charging demands at FCS and CP can generally be obtained from operators equipped with advanced metering infrastructure, the situation is more complex in residential settings. Home smart meters typically record aggregated electricity consumption, which includes other household appliances alongside EV charging. Therefore, the EV charging load from residential wall outlets must be disaggregated from the total consumption [16, 17].

Given the strong interdependence between these two subtasks, a multi-task learning architecture can effectively leverage shared information to enhance overall monitoring accuracy. This is implemented by using shared lower layers to capture general features, with individual task-specific tower layers built on top of these shared representations [16, 17].

Task 1. State detection: The goal is to determine whether an EV is in a charging or idle state (denoted s_t) by analyzing the observed aggregated load time series $\tilde{\mathbf{Y}}$ (i.e., mapping $\tilde{\mathbf{Y}}$ to s_t).

Task 2. Load disaggregation: Here, the primary focus is tracking the EV charging power, while treating the power consumed by all other appliances as background noise (mapping $\tilde{\mathbf{Y}}$ to $\tilde{x}_t^{EV}$). This relationship is expressed as:

$$\tilde{y}_t = \tilde{x}_t^{EV} + \sum_{a \neq EV} \tilde{x}_{a,t} + e_t = \tilde{x}_t^{EV} + \varepsilon_t \tag{20}$$

For the state detection task, the loss function is formulated as (21):

$$\mathcal{L}_s = -\frac{1}{T}\sum_{t=1}^{T}\begin{pmatrix} s_t \log\left(\hat{s}_t \mid \tilde{\mathbf{Y}}, \theta_S, \theta_T\right) \\ +(1-s_t)\log\left(1-\hat{s}_t \mid \tilde{\mathbf{Y}}, \theta_S, \theta_T\right) \end{pmatrix} \tag{21}$$

where $(\cdot)$ denotes the predicted output, θ_S represents the parameters of the shared layers, and θ_{T} denotes the parameters of the state-detection-specific tower.

For load disaggregation, the loss function can be expressed as (22).

$$\mathcal{L}_d = \frac{1}{T}\sum_{t=1}^{T}\left(\tilde{x}_t^{EV} - \left(\hat{x}_t^{EV} \mid \tilde{\mathbf{Y}}, \theta_S, \theta_D\right)\cdot\left(\hat{s}_t \mid \tilde{\mathbf{Y}}, \theta_S, \theta_T\right)\right)^2 \tag{22}$$

where θ_D is the parameter of the load disaggregation tower.

It should be emphasized that this formulation in (22) differs from the standard mean squared error (MSE) because the EV consumes zero power during idle periods. Thus, the output charging power satisfies $\hat{x}_t^{EV,out} = \hat{x}_t^{EV} \cdot \hat{s}_t$.

Once the home wall-outlet EV charging power ($\hat{x}_t^{EV,out}$*) has been successfully disaggregated from the readings of the smart meter, the aggregate EV charging power at bus i (*$P_{i,t}^{EV}$) can be obtained by summing the contributions from all charging sources within the corresponding area.

3. Experiments

3.1 Experimental Setup

Load curves, units output curves and EV charging curves and electricity prices are taken from a report by the Economic and Technical Research Institute of the State Grid Electric Power Co., Ltd. All case studies were implemented using Gorubi, Yalmip and Cplex on a computer with AMD R7-6800 CPU and 16 GB RAM.

3.2 Benchmarks and index

In the distribution network analyzed in this study, there are no distributed power sources; all electricity consumed by users is purchased entirely from the upstream grid.

Figure 2: Optimized electricity price

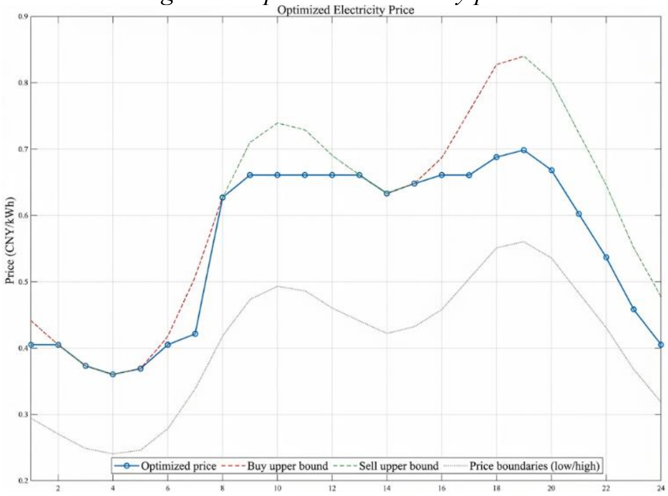

Figure 2 shows two peak-valley differences in a single day, with 2 peaks at 10 and 19, and 2 valleys at 4 and 14. The optimized electricity price maintains a consistent trend.

Figure 3: EV charging power by type

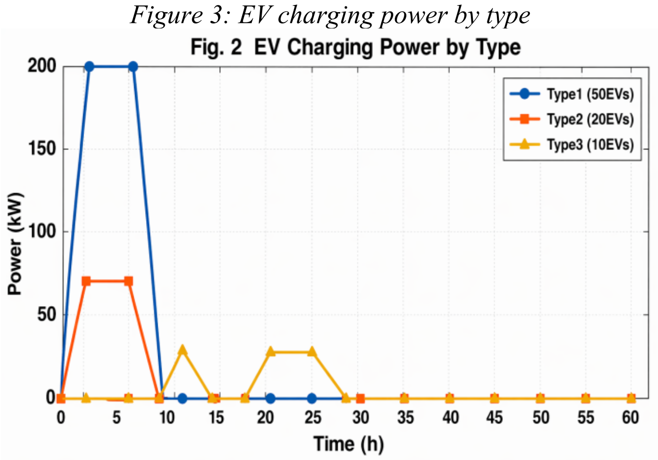

In Figure 3, for type 1, charging is implemented from 12:00 a.m. to 6:00 a.m. due to low price of valley electricity. For type 2, it has the same interval of peak charging power as type 1 while its peak value is lower than type 1's. Type 3 is not so regulated as the other 2 types. The charging occurs in the morning (7–9). That may be due to some unexpected accidents.

In Figure 4, the blue bars over the horizontal line aligned with zero power means charging while the orange bars underneath that line means discharging. If the line chart is found horizontal in certain interval, there is no charging or discharging during that period. The future renewable energy installation and load data are taken from a report by the Economic and Technical Research Institute of the State Grid Electric Power Co., Ltd.

In Figure 5, the sale electricity price is determined by the volume of real-time electricity trading. The orange bars is the real-time price of sale, which is equal to the price of purchase electricity. The blue chart means the optimized price at every time, which shows 1 valley in the morning (4 a.m.) and 1 peak in the evening (7:00 p.m.).

3.3 Results and Analysis

In Figure 6, the blue chart means the electricity load curve at every time and the red one implies the dynamic marginal carbon emission factors. The blue chart shows an obvious peak at 12 while the red one shows a valley from 9 to 15, during which the output of photovoltaic and wind power increases. However, the output of fossil fuel decreases during that time. As a result, during the same period the MEF becomes the lowest period in a typical day. During the other period, the MEF is higher since there is less the output of photovoltaic and wind power, so that the output of fossil fuel is much more relied.

Figure 4: Energy storage operation

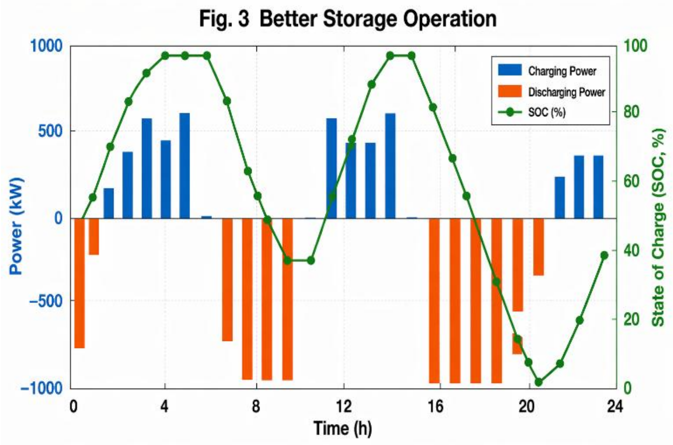

Figure 5: Real-time electricity trading and price.

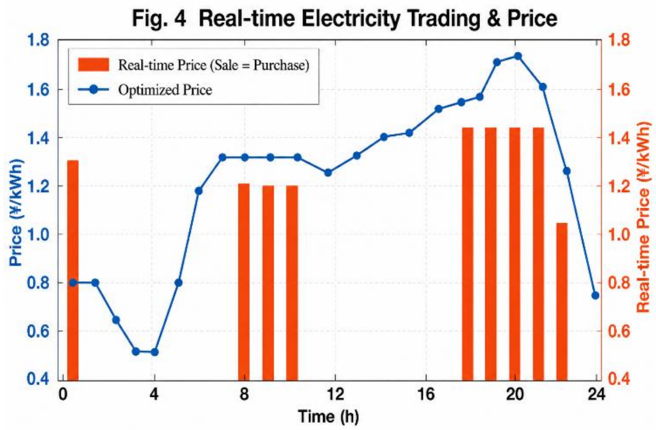

Figure 6: Dynamic marginal carbon emission factor (MEF).

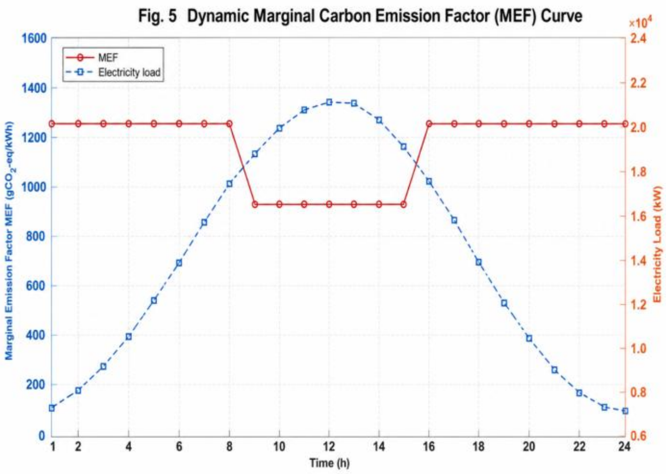

Figure 7: Dynamic carbon emission factors (XEF and MEF)

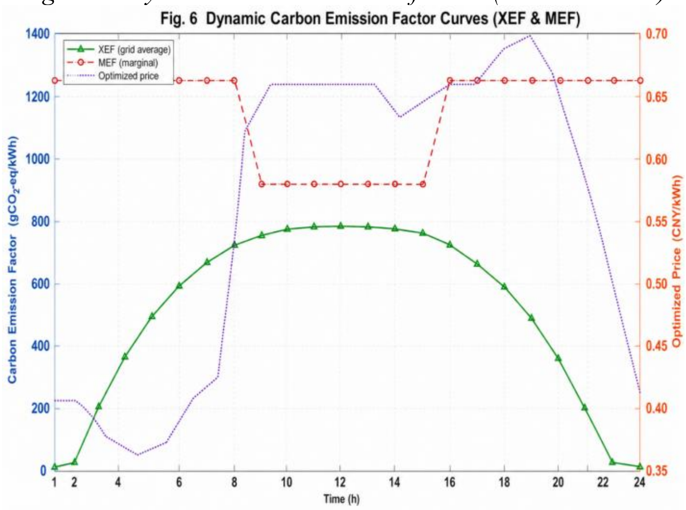

Figure 7 is a combination of the red chart of MEF in Figure 6 and the blue chart of optimized price in Figure 5 with a new green chart of XEF. It increases and then decreases in a day with a maximum point when it is at 12:00 p.m. According to (11), XEF can be affected by fossil fuel consumption and fossil emission factor. From 00:00 to 08:00, XEF increases violently because the power consumption in this period are lower than that at noon. Moreover, no one uses electricity initially and the output of photovoltaic and wind power is also less than that at noon. So, most of the output is from fossil fuel during that period. As power consumption increases, the usage of fossil fuel also increases, which leads to a rise in XEF. From 09:00 to 17:00, the power consumption becomes higher since the legal working hours are from 09:00 to 17:00. There are more industrial and commercial activities, which lead to a rise in power consumption. Finally, from 18:00 to 23:00, the output of photovoltaic power turns less along with a rise in residential power consumption. However, residential power consumption is just 1/3 of industrial one.

4. Conclusion

In this paper, the issue of user-side low-carbon scheduling for electric vehicles is investigated through the construction of a framework integrating dynamic electricity pricing, energy storage system operation, EV charging patterns, and dynamic carbon emission factors. The study reveals that although electric vehicles do not emit direct exhaust gases during operation, indirect carbon emissions can still occur during charging depending on the electricity source. Hence, EV scheduling should consider not only electricity costs but also the carbon emission profile of the power system.

Experimental results show that dynamic electricity pricing can guide electric vehicles to shift charging loads toward valley periods, while energy storage systems can improve load distribution through valley charging and peak discharging. At the same time, the dynamic carbon emission factor curves indicate that low-electricity-price periods do not necessarily correspond to low-carbon periods, as carbon emission levels are also influenced by renewable energy output and the proportion of fossil energy generation.

Consequently, user-side low-carbon scheduling of electric vehicles should comprehensively consider both electricity price signals and carbon emission signals. The integration of dynamic electricity prices, energy storage operation, and carbon emission factors can more effectively reduce indirect EV carbon emissions and enhance the low-carbon capability and flexibility of power system operation.

References

[1] Algarni, A. S., Suryanarayanan, S., Siegel, H. J., & Maciejewski, A. A. (2021). Combined impact of demand response aggregators and carbon taxation on emissions reduction in electric power systems. *IEEE Transactions on Smart Grid, 12*(2), 1825-1827.

[2] Fabbri, G., Odoardi, S., Tarquini, G., Pasquali, L., Teodori, S., & Santini, E. (2014). Impact of V2G/G2V technologies on distributed generation systems. *Proceedings of the IEEE 23rd International Symposium on Industrial Electronics*, 1677-1682.

[3] Kang, C., Zhou, T., Chen, Q., Xu, Q., Xia, Q., & Ji, Z. (2015). Carbon emission flow from generation to demand: A network-based model. *IEEE Transactions on Smart Grid, 6*(5), 2386-2394.

[4] Kang, C., Zhou, T., Chen, Q., Xu, Q., Xia, Q., & Ji, Z. (2012). Carbon emission flow in networks. *Scientific Reports, 2*, Article 479.

[5] Li, B., Song, Y., & Hu, Z. (2013). Carbon flow tracing method for assessment of demand-side carbon emissions obligation. *IEEE Transactions on Sustainable Energy, 4*(4), 1100-1107.

[6] Li, D., Chiu, W.-Y., Sun, H., & Poor, H. V. (2018). Multiobjective optimization for demand side management program in smart grid. *IEEE Transactions on Industrial Informatics, 14*(4), 1482-1490.

[7] Lu, Z., Bai, L., Wang, J., Wei, J., Xiao, Y., & Chen, Y. (2023). Peer-to-peer joint electricity and carbon trading based on carbon-aware distribution locational marginal pricing. *IEEE Transactions on Power Systems, 38*(1), 835-852.

[8] Mahmoud, M. S., Rahman, M. S. U., & Al-Sunni, F. M. (2015). Review of microgrid architectures: A system of systems perspective. *IET Renewable Power Generation, 9*(8), 1064-1078.

[9] Mu, C., Ding, T., Zhu, S., Han, O., Du, P., Li, F., & Siano, P. (2023). A decentralized market model for a microgrid with carbon emission rights. *IEEE Transactions on Smart Grid, 14*(2), 1388-1402.

[10] Nguyen, H. N., Zhang, C., & Mahmud, M. A. (2015). Optimal coordination of G2V and V2G to support power grids with high penetration of renewable energy. *IEEE Transactions on Transportation Electrification, 1*(2), 188-195.

[11] Qiu, J., Dong, Z. Y., Zhao, J., Xu, Y., Luo, F., & Yang, J. (2016). A risk-based approach to multi-stage probabilistic transmission network planning. *IEEE Transactions on Power Systems, 31*(6), 4867-4876.

[12] Rodrigues, Y. R., de Souza, A. C. Z., & Ribeiro, P. F. (2018). An inclusive methodology for plug-in electrical vehicle operation with G2V and V2G in smart microgrid environments. *International Journal of Electrical Power & Energy Systems, 102*, 312-323.

[13] Tao, Y., Qiu, J., Lai, S., Wang, Y., & Sun, X. (2023). Reserve evaluation and energy management of microgrids in joint electricity markets based on non-intrusive load monitoring. *IEEE Transactions on Industry Applications, 59*(1), 207-219.

[14] Wang, X., Gong, Y., & Jiang, C. (2015). Regional carbon emission management based on probabilistic power flow with correlated stochastic variables. *IEEE Transactions on Power Systems, 30*(2), 1094-1103.

[15] Wang, Y., Qiu, J., Tao, Y., Zhang, X., & Wang, G. (2020). Low-carbon oriented optimal energy dispatch in coupled natural gas and electricity systems. *Applied Energy, 280*, Article 115948.

[16] Yan, M., Shahidehpour, M., Alabdulwahab, A., Abusorrah, A., Gurung, N., Zheng, H., Ogunmubi, O., Vukojevic, A., & Paaso, E. A. (2021). Blockchain for transacting energy and carbon allowance in networked microgrids. *IEEE Transactions on Smart Grid, 12*(6), 4702-4714.

[17] Zhuang, M., Shahidehpour, M., & Li, Z. (2018). An overview of non-intrusive load monitoring: Approaches, business applications, and challenges. *Proceedings of the IEEE International Conference on Power System Technology*, 4291-4299.

Funding

This research received no external funding.

Conflicts of Interest

The authors declare no conflict of interest.

Acknowledgment

This paper is an output of the science project.